JARO 2/1: 065–071 (2001)
DOI: 10.1007/s101620010041

JARO
Journal of the Association for Research in Otolaryngology

Keratin Particle-Induced Osteolysis: A Mouse Model of Inflammatory Bone Remodeling Related to Cholesteatoma

RICHARD A. CHOLE,[1,2] RUTH M. HUGHES,[1] AND BRIAN T. FADDIS[1]

[1]*Department of Otolaryngology, Washington University School of Medicine, St. Louis, MO 63110, USA*
[2]*Department of Molecular Pharmacology, Washington University School of Medicine, St. Louis MO 63110, USA*

Received: 13 April 2000; Accepted: 14 November 2000; Online publication: 16 March 2001

ABSTRACT

We implanted keratin and poly(methyl methacrylate) (PMMA) particles to the surface of mouse calvariae to produce a quantitative, localized, inflammatory bone remodeling similar to that seen in cholesteatoma. Both types of particles resulted in increased osteoclast density compared with controls. Osteoclasts infiltrated from marrow and vascular spaces and were active at the periphery of these spaces leading to significant bone remodeling, as demonstrated by the incorporation of bone-labelling fluorophores. Osteoclasts were rarely found on the surface of the calvariae, and mineral apposition rate at the ventral surface was not altered in keratin-implanted animals compared with nonoperated controls. While not useful for the study of the root cause of cholesteatoma, this model will allow the study of pathologic bone remodeling related to cholesteatoma in a genetically defined animal.

Keywords:

INTRODUCTION

Acquired aural cholesteatomas arise from the keratinizing epithelium from the lateral surface of the tympanic membrane as a result of otitis media or trauma. Once established, entrapped keratin accumulates within the cholesteatoma. The enlarging cholesteatoma often becomes chronically infected and has a propensity to erode surrounding bone leading to hearing loss, vestibular damage, and even intracranial invasion.

The study of human cholesteatoma, its development and pathophysiology, has been advanced by a number of animal models of the disease. Except for the human, the only animals known to develop cholesteatomas spontaneously are the Mongolia gerbil, *Meriones unguiculatus* (Chole et al. 1981) and the fat sand rat, *Psommamys obesus* (Feinmesser et al. 1988). The Mongolian gerbil develops aural cholesteatomas with age but they can be accelerated by the ligation of the external auditory canal (McGinn et al. 1982). Furthermore, blockage of the eustachian tube in gerbils lead to retraction of the pars flaccida in a manner identical to human primary acquired cholesteatomas (Wolfman and Chole 1986; Kim and Chole 1998). Other models of cholesteatoma in the chinchilla (Wright et al. 1985; Wright and Meyerhoff 1988) and the rat (Schmidth and Hellstrom 1994) offer additional important tools for the study of this disease. While each of these models mimics the human condition, studies using these models are limited by the paucity of genetic information in these species. The purpose of this study was to develop a model in which the bone-resorbing characteristics of cholesteatomas could be studied in a mouse model. Many of the genes and their products that control the inflammatory process are well characterized in mice. Furthermore, the genes of many of these mediators have been selectively altered yielding knockout and transgenic mice which are available for study.

Cholesteatomas do not occur spontaneously in mice

Correspondence to: Dr. Richard A. Chole • Department of Otolaryngology • Washington University School of Medicine • Campus Box 8115 • 660 South Euclid Avenue • St. Louise, MO 63110. Telephone: (314) 362-7395; fax: 314; 747-1004; email: choler@msnotes.wustl.edu

and they cannot be induced by ear canal ligation or eustachian tube obstruction (McGinn et al. 1984). We developed a strategy that combines the findings of Moriyama and colleagues (1984), who showed that keratin implanted subcutaneously leads to chronic inflammation, and Merkel and colleagues (1999), who developed a murine model of particle-induced bone resorption. We implanted keratin particles onto the calvarium of mature mice and induced bone resorption and remodeling.

METHODS AND MATERIALS

Experimental design

Forty-two young adult (6–7 week) C57BL/6 mice, *Mus musculus*, were used in this study. Twelve animals were used for each of three different survival periods. Within each survival group, four experimental conditions were randomly assigned to half calvaria: (1) Control—no manipulation; (2) Sham control—periosteum lifted and replaced; (3) implantation poly-(methyl methacrylate) (PMMA) particles (Merkel et al. 1999); and (4) implantation of human keratin particles. Additionally, four mice were implanted with murine keratin reconstituted from the nails and fur from C57BL/6 mice. Animals were sacrificed at 7, 14, and 28 days post-treatment. This study was performed in accordance with the PHS Policy on Humane Care and Use of Laboratory Animals, the NIH *Guide for the Care and Use of Laboratory Animals*, and the Animal Welfare Act (7 U.S.C. *et seq.*). The animal use protocol was approved by the Institutional Animal Care and Use Committee (IACUC) of Washington University.

Materials

Keratin was obtained from human and murine sources. Human keratin particles were derived from fingernail filings of volunteers. These particles, which ranged in diameter from 5 to 50 μm, were sterilized in ethylene oxide for 2 hours prior to implantation. Murine keratin was also derived from ground nails or extracted from hair from C57BL/6 mice using the protocol described by Yamauchi et al. (1996). Briefly, hair keratin was solubilized in a solution containing 5.6M urea, 2.7% SDS (w/v) and 6.7% (v/v) 2-mercaptoethanol at neutral pH for 12 hours. The extract was dialyzed against 0.08% mercaptoethanol in water (3.5 L, 3 times) to yield a colorless and dessicated to a dry powder and sterilized in ethylene oxide for 2 hours prior to implantation. SDS-PAGE analysis of the extracted keratin was consistent with the known molecular weight range of keratins, approximately 45–70 kD.

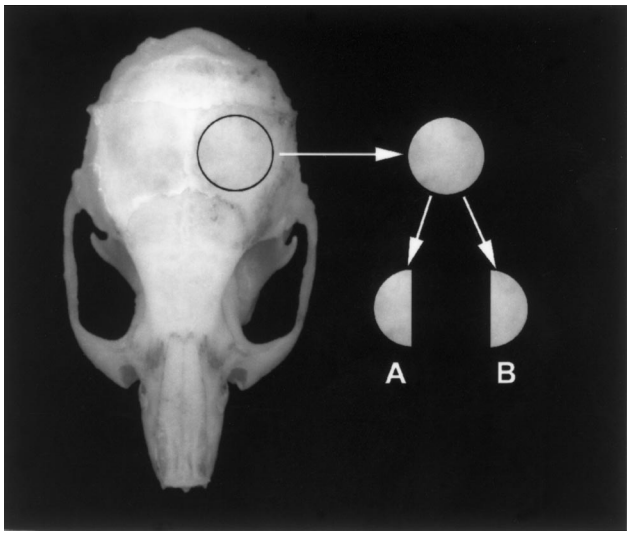

FIG. 1. Photograph of a representative mouse calvarial surface. A 4.0-mm biopsy punch (circle) was excised form parietal bone with care taken to avoid the sagittal suture. Each punch was then halved and processed for histomorphometic (**A**) and mineral apposition rate (**B**) studies.

Sterile PMMA particles were a gift of Wright Medical Technologies (Arlington, TN).

Treatment protocol

Each animal was anesthetized with methoxyflurane (Metofane®, Schering-Plough, Kenilworth, NJ) and the surgical site was shaved and sterilized with iodine. A linear incision was made through the skin over the dorsum of the head, the skin was retracted laterally, and the periosteum was elevated from the parietal bone. The experimental material was placed onto the exposed bone and the incision closed with a sterile wound clip.

Two fluorochromes were used to allow the measurement of mineral apposition rate (MAR). These fluorochromes were administered at the beginning and end of the 1-week survival group, at day 8 and day 14 of the 2-week survival group, and at day 22 and day 28 of the 4-week survival group. This would allow us to observe MAR during a variety of week-long intervals post-treatment. Tetracycline (24 mg/kg) in sterile phosphate-buffered saline (PBS) was administered at the beginning of the period of interest. Calcein blue (32 mg/kg, in sterile PBS) was administered approximately 6 hours prior to sacrifice. The fluorochromes were administered by intraperitoneal injection; injection volume did not exceed 0.2 mL. All mice received food and water *ad libitum* and were maintained on a 12/12 light–dark cycle to avoid disruption of circadian rhythm patterns.

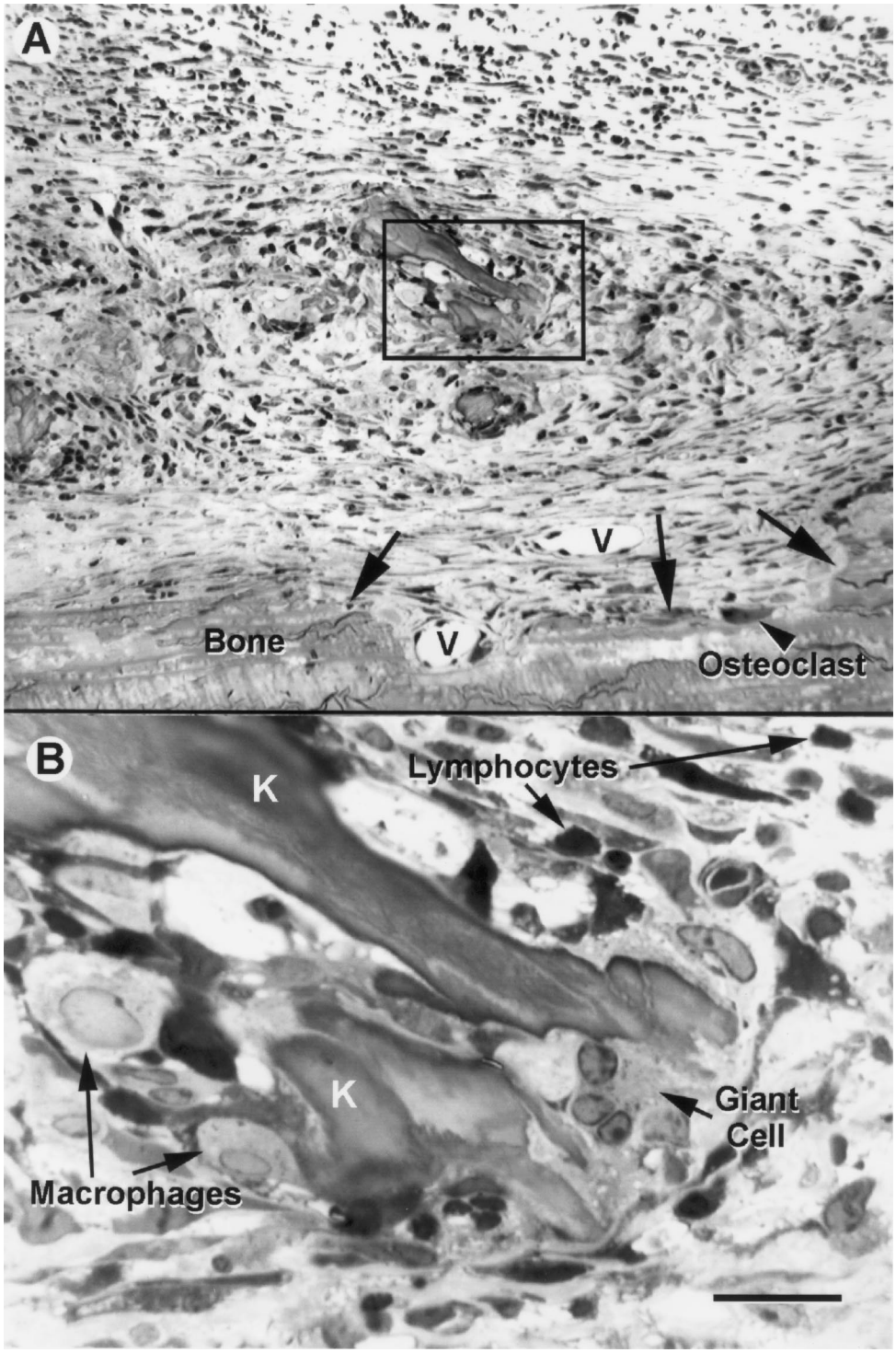

FIG. 2. A. Inflammatory response typical of the site of keratin implant at 1 week survival. The irregular surface of the bone (arrows) is suggestive of erosion though few surface osteoclasts are seen at this time. New vessels (v) are evident and, at higher power (inset, **B**) the remains of keratin debris (k) can be seen surrounded by macrophages, lymphocytes, and giant cells. Scale bar = 25 μm.

Histology

At the end of the experimental period, the animals were euthanized with pentobarbital (>200 mg/kg). The calvarium was exposed and the parietal bones removed. A 4.0-mm biopsy punch was excised from each parietal bone and fixed overnight in a phosphate-buffered solution containing 4% paraformaldehyde and 0.05% glutaraldehyde (Fig. 1). The following day, bone samples were cut in half with one portion placed into 0.35M tetrasodium EDTA (pH 7.4) for several days. These specimens were then dehydrated in graded solutions of acetone and embedded in an epon-araldite resin. One-micrometer-thick sections were collected and stained with toluidine blue and basic fuchsin.

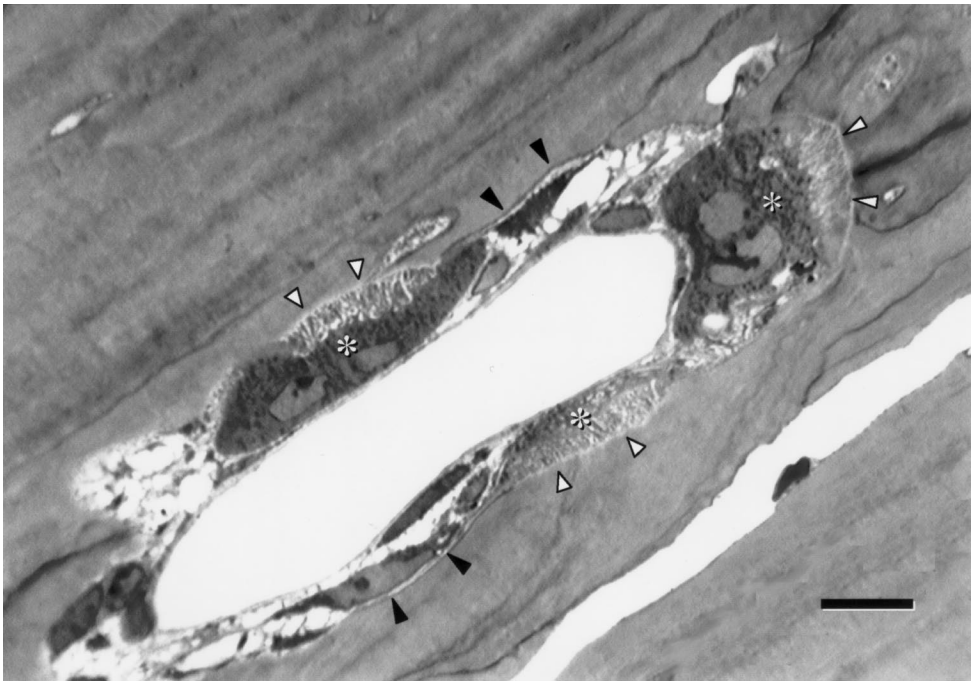

FIG. 3. Photomicrograph of a vascular space within a calvaria implanted with keratin particles and harvested at 7 days post-implant. Three typical osteoclast profiles (*) are seen which exhibit granular cytoplasm and robust ruffled borders (white arrowheads) where the cells are apposed to bone. Two of the profiles are multinucleated. In addition, the darkly stained lamina limitans (black arrowheads) is absent in areas in contract with the osteoclast ruffled border. Scale bar = 10 μm.

Osteoclast counts

The experimenter performing counts of osteoclasts was blinded as to the experimental treatment. Using an Olympus® BH microscope, osteoclasts were identified and counted for each hemisphere, avoiding the region immediately adjacent to the sagittal suture. To be counted as an osteoclast, a cellular profile had to be localized adjacent to bone and had to demonstrate at least three of the following four criteria: (1) ruffled border, (2) granular cytoplasm, (3) multiple nuclei ($\geq$2), and (4) absence of a lamina limitans along some surface of the bone in contact with the cell profile. Osteoclast number (total number of osteoclasts/total mm bone length, N.Oc/TL) was quantitated using a SigmaScan Pro® image analysis system (SPSS Science Inc., City, State). Osteoclast counts were averaged from three sections per animal; sections were spaced at 100 μm to avoid counting the same cell more than once. Halving the biopsy punch provided a uniform 4-mm length of bone which was verified and adjusted as necessary.

Mineral apposition rate

The remaining half of the parietal bone biopsy punches were dehydrated in graded solutions of ethanol or acetone and embedded in Spurr's resin. Thin saw-cut slices from these tissues were glued to glass microscope slides with cyanoacrylate, sanded to a final thickness of approximately 10 μm, coverslipped with nonfluorescing immersion oil, and viewed with epifluorescence utilizing UV wavelength excitation. Both fluorochromes were visible simultaneously under these conditions. Digital images were captured from two separate regions of each hemisphere, and total mineral apposition was calculated as the average total area between the two labels. Mineral apposition rate (MAR, μm/day) was calculated as this mean area divided by the labeling interval of 7 days.

Statistics

The data were analyzed using one-way analysis of variance (ANOVA) for independent groups followed by Duncan's multiple comparison test (SigmaStat, SPSS Science Inc.). In all analyses, $\alpha = 0.05$.

RESULTS

Keratin (human and murine) and PMMA implantation resulted in a localized inflammatory response with the accumulation of macrophages and lymphocytes (see Fig. 2). Macrophages were most plentiful around particles. Multinucleate giant cells were frequently seen. Blood vessel proliferation was prominent after 1 week but was not as obvious after 2 and 4 weeks. Keratin and PMMA particles were more plentiful at 1 week than at 2 and 4 weeks suggesting that the implanted particles are removed by the action of macrophages and giant cells. Osteoclast profiles were easily identified based on our selection criteria (see Fig. 3). These were typically very plump cells with prominent ruffled borders and granular cytoplasm. The vast majority of osteoclasts were found at the periphery of the calvarial marrow and vascular spaces. Profiles of

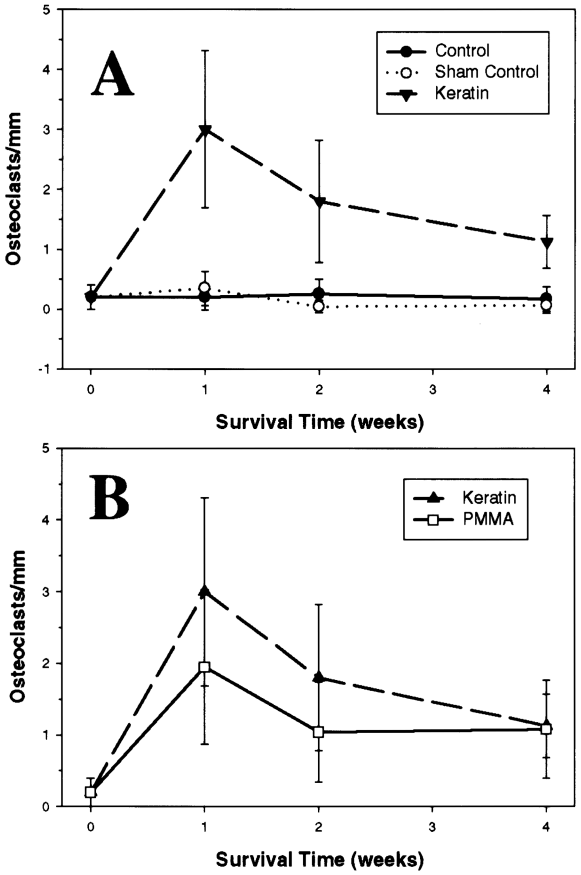

FIG. 4. Histograms depicting means and standard deviations of osteoclast counts per millimeter of bone length. **A.** Implantation of keratin particles (▲) leads to an increase in osteoclast number within 1 week ($p < 0.001$), followed by a steady decline in subsequent weeks ($p < 0.05$). Non-operated (●) and sham-operated (○) controls showed no change in osteoclast density over course of the study. **B.** Osteoclast activation induced by PMMA (■) was not significantly different in magnitude to that of the keratin group (▲).

other multinucleated cells, i.e., megakaryocytes and foreign body giant cells, were also found in these spaces but did not exhibit the selection criteria and were not counted as osteoclasts. Most of the counted profiles exhibited more than one nucleus, some as many as eight. Very few osteoclasts were found on the dorsal surface of the calvarium and usually these seemed to result from complete degradation of the bone between the marrow space and the calvarial surface. No osteoclasts were observed on the ventral surface of the calvarium.

Keratin and PMMA particles implanted on the surface of the murine calvarium lead to the activation of osteoclasts in the adjacent bone in a manner similar to that seen in human cholesteatomas (Chole 1984) and in particle-induced osteolysis (Merkel et al. 1999). A significant increase in osteoclast number was seen in keratin implants compared with unoperated and sham controls at all time periods examined (Fig. 4A). Osteoclast number density from keratin and PMMA implants did not differ significantly at any time period (see Fig. 4B). Keratin, but not PMMA implants, exhibited a decrease in osteoclast number from 1 to 4 weeks postimplant.

Mouse keratin was used in four additional animals to rule out the possibility that the inflammatory response and osteoclast recruitment were due to a hypersensitivity reaction caused by the use of foreign protein (human keratin). These animals were sacrificed at 1 week postimplant and demonstrated osteoclast recruitment comparable to those animals receiving human keratin. In addition, there were no qualitative differences in the cellular response to reconstituted murine keratin when compared with human keratin.

Both fluorochromes were evident only in tissues harvested at 1 week post-treatment. Furthermore, the double label in these tissues was only evident at the ventral surface of the calvarium. Tetracycline labeling did demonstrate a pronounced increase of mineral apposition around the marrow spaces at 2 weeks that returned to normal by 4 weeks postimplant. Mineral apposition rates at the ventral surface did not differ between any of the experimental groups at 1 week survival (see Fig. 5).

DISCUSSION

Human cholesteatomas lead to a chronic inflammatory process within the middle ear and mastoid, which commonly leads to localized bone resorption. The resorption of bone in human cholesteatoma is due to the recruitment and activation of osteoclasts (Chole 1984; Uno and Saito 1995). Osteoclast activation occurs as a result of factors produced in the vicinity of the inflammatory response. Among other factors, the presence of keratin itself, with and without infection, leads to chronic inflammation (Moriyama et al. 1984; Iino et al. 1990a,b). Several observers have shown that some cholesteatomas can cause chronic inflammation by the extravasation of keratin debris (Kaneko et al. 1980; Abramson et al. 1984). By implanting keratin particles onto the calvarial surface of the mouse, we have shown a process that is similar to that seen in human cholesteatomas: a chronic inflammatory response with angioneogenesis, mononuclear cell recruitment, and osteoclast and osteoblast activation with bone resorption and deposition.

The current study utilized a bilateral design, which allowed two treatments within the same animal. Although the data confirm that osteoclast numbers in control tissues are minimal, we did routinely observe some displacement of the keratin or PMMA particles from the experimental side to the contralateral control

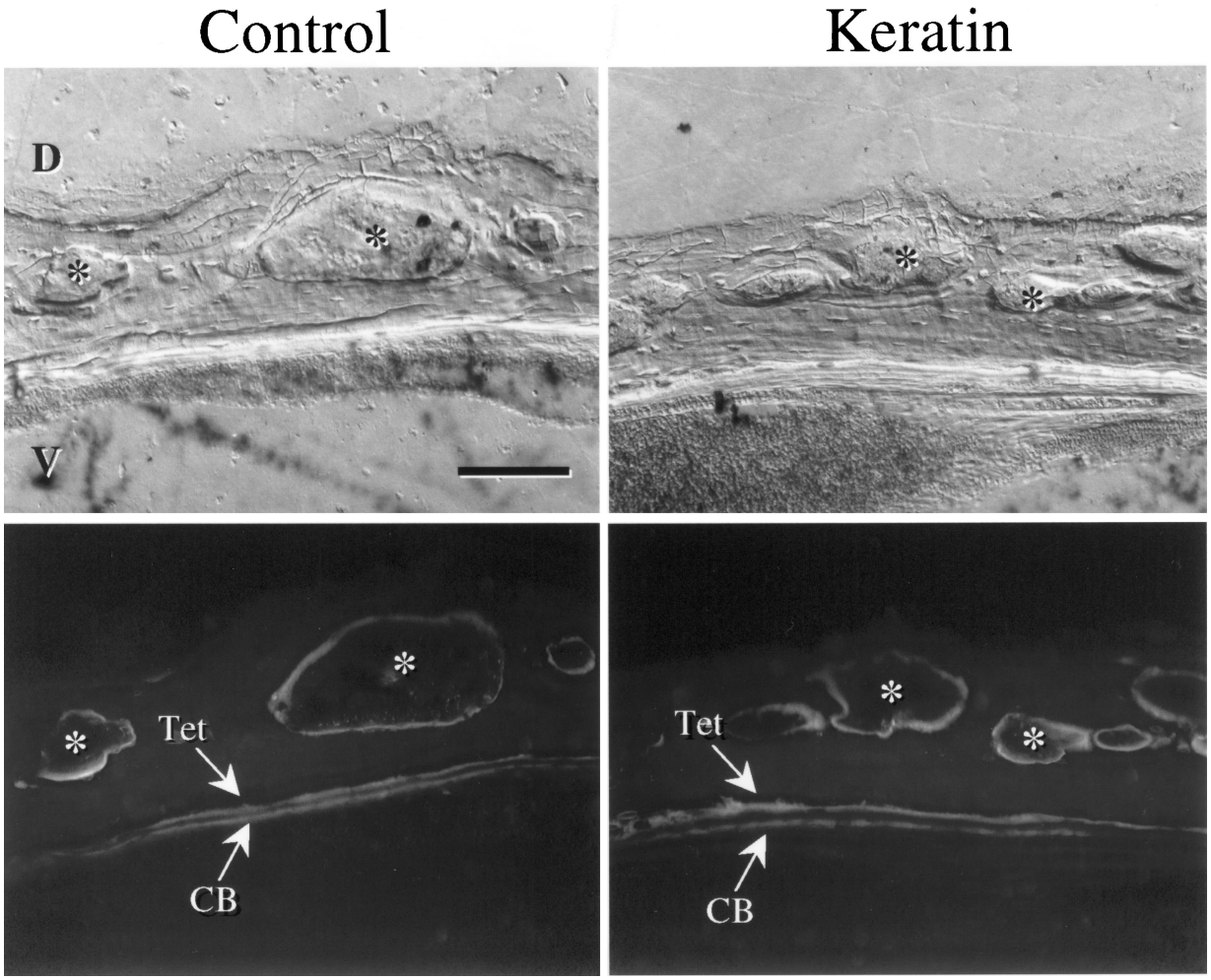

FIG. 5. Nomarski (upper panels) and fluorescent (lower panels) images clearly demonstrate the localization of the bone-incorporated fluorophores, tetracycline (Tet) and calcein blue (CB), at the ventral surface (V) of the calvariae during the first week following keratin implantation. Clear labels were produced by both fluorophores, which could be visualized simultaneously using UV excitation. Additional tetracycline label was seen at the periphery of the marrow spaces (*), but double labeling was not routinely evident here. No labeling was appreciable at the dorsal surface of the clavariae (D). The area between the two labels was measured and divided by the length to yield an estimate of the average apposition in micrometers. Scale bar = 100, μm.

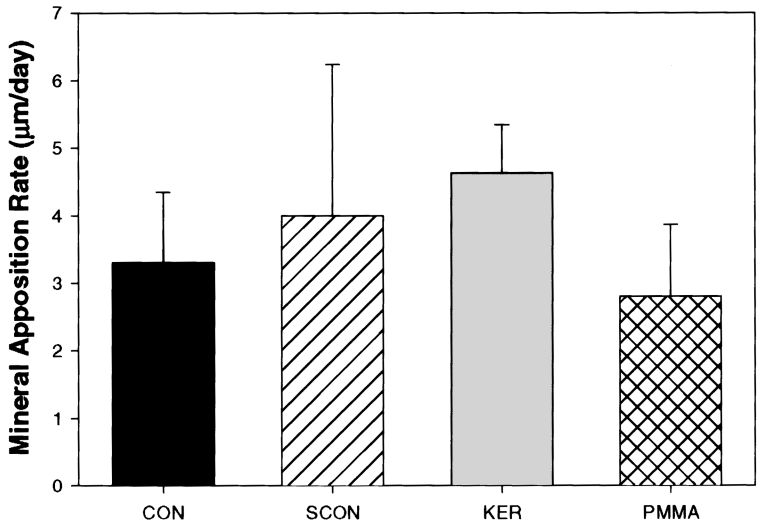

FIG. 6. Histogram depicting means and standard deviations of mineral apposition rates of the four groups measured μm/day. Fluorochrome labeling studies revealed no difference in MAR at the ventral calvarial surface between any of the groups measured.

side. An earlier pilot study, which minimized the amount of implant substance to control for this contamination, resulted in an absence of osteoclast activation with keratin or PMMA implants (data not shown). Since the amount of substance implanted can so directly affect osteoclast activation, we propose to use separate matched animals for control and experimental treatments in future studies. We also observed significant interanimal variability in the amount of clearing of the implanted substance. This may have been due to displacement caused by handling or animal movement or a physiologic removal by macrophages. Whatever the mechanism, premature clearing could most certainly affect the degree or duration of osteoclast activity and we would therefore propose to optimize the amount of substance implanted in future studies. Also, at 1 week we may have already missed the peak period of osteoclast density. In support of this notion, several tissues showed evidence of significant bone remodeling but with very few osteoclasts present at 1 week postimplant. It is clear that it will be necessary to reduce this variability or increase the sample size for future studies.

Surprisingly, very few osteoclasts were found on the dorsal surface of the calvarium. This may be due to the proximity of the calvarial marrow spaces, which are a ready source of osteoclast precursors. The bilateral design used proves that implanted keratin or PMMA is exerting a very localized effect with regard to osteoclast activation. Perhaps signals of osteoclast activation are diffusing to the marrow spaces and initiating osteoclast development and activation at this site. Future studies will attempt to identify some of these signals and the temporal course of their action.

The described model of localized inflammatory bone remodeling will allow study of the processes by which cholesteatomas cause bone resorption and deposition in a genetically well-defined animal. This model will be useful for the study of the pathological processes related to cholesteatoma but it is not useful for the study of the processes by which cholesteatomas arise. The spontaneous and induced models in gerbils (Chole et al. 1981; McGinn et al. 1982; Wolfman and Chole 1986) and sand rats (Feinmesser et al. 1988) are more appropriate for study of the pathogenesis of this disease.

ACKNOWLEDGMENT

Special thanks to Jae Jung for preparation of mouse keratin. Supported by a grant from the National Institutes of Health (R01-DC00263) (RAC).

REFERENCES

ABRAMSON M, MORIYAMA H, HUANG CC. Pathogenic factors in bone resorption in cholesteatoma. Acta Otolaryngol. (Stockh.) 97:437–442, 1984.

CHOLE RA. Cellular and subcellular events of bone resorption in human and experimental cholesteatoma: the role of osteoclasts. Laryngoscope 94:76–95, 1984.

CHOLE RA, HENRY KR, MCGINN MD. Cholesteatoma: spontaneous occurrence in the Mongolian gerbil *Meriones unguiculatis*. Am. J. Otol. 2:204–210, 1981.

FEINMESSER R, UNGAR H, ADLER J. Otic cholesteatoma in the sand rat (*Psammomys obesus*). Am. J. Otol. 9:409–411, 1988.

IINO Y, TORIYAMA M, OGAWA H, KAWAKAMI M. Cholesteatoma debris as an activator of human monocytes. Potentiation of the production of tumor necrosis factor. Acta Otolaryngol. (Stockh.) 110:410–415, 1990a.

IINO Y, TORIYAMA M, OHMI S, KANEGASAKI S. Activation of peritoneal macrophages with human cholesteatoma debris and alpha-keratin. Acta Otolaryngol. (Stockh.) 109:444–449, 1990b.

KANEKO Y, YUASA R, ISE I. Bone destruction due to the rupture of a cholesteatoma sac: a pathogenesis of bone destruction in aural-cholesteatoma. Laryngoscope 90:1865–1871, 1980.

KIM HJ, CHOLE RA. Experimental models of aural cholesteatomas in Mongolian gerbils. Ann. Otol. Rhinol. Laryngol. 107:129–134, 1998.

MCGINN MD, CHOLE RA, HENRY KR. Cholesteatoma. Experimental induction in the Mongolian Gerbil, *Meriones unguiculatis*. Acta Otolaryngol. (Stockh.) 93:61–67, 1982.

MCGINN MD, CHOLE RA, HENRY KR. Cholesteatoma induction. Consequences of external auditory canal ligation in gerbils, cats, hamsters, guinea pigs, mice and rats. Acta Otolaryngol. (Stockh.) 97:297–304, 1984.

MERKEL KD, ERDMANN JM, MCHUGH KP, ABU-AMER Y, ROSS FP, TEITELBAUM SL. Tumor necrosis factor-alpha mediates orthopedic implant osteolysis. Am. J. Pathol. 154:203–210, 1999.

MORIYAMA H, HUANG CC, SHIRAHATA Y, ABRAMSON M. Effects of keratin on bone resorption in experimental otitis media. Arch. Otorhinolaryngol. 239:61–68, 1984.

SCHMIDT SH, HELLSTROM S. Experimental cholesteatoma in the rat. Acta Otolaryngol. (Stockh.) 114:430–434, 1994.

UNO Y, SAITO R. Bone resorption in human cholesteatoma: morphological study with scanning electron microscopy. Ann. Otol. Rhinol. Laryngol. 104:463–468, 1995.

WOLFMAN DE, CHOLE RA. Experimental retraction pocket cholesteatoma. Ann. Otol. Rhinol. Laryngol. 95:639–644, 1986.

WRIGHT CG, MEYERHOFF WL. Cholesteatoma can be produced in experimental animals by the application of topical antibiotic drops to middle ear (letter). Am. J. Otolaryngol. 9:341, 1988.

WRIGHT CG, MEYERHOFF WL, BURNS DK. Middle ear cholesteatoma: an animal model. Am. J. Otolaryngol. 6:327–341, 1985.

YAMAUCHI K, YAMAUCHI A, KUSUNOKI T, KOHDA A, KONISHI Y. Preparation of stable aqueous solution of keratins, and physiochemical and biodegradational properties of films. J. Biomed. Mat. Res. 31:439–444, 1996.